Molecular Therapy
Nucleic Acids
Original Article

# Inhibition of EGF Uptake by Nephrotoxic Antisense Drugs In Vitro and Implications for Preclinical Safety Profiling

Annie Moisan,[1] Marcel Gubler,[1] Jitao David Zhang,[1] Yann Tessier,[2] Kamille Dumong Erichsen,[2] Sabine Sewing,[1] Régine Gérard,[1] Blandine Avignon,[1] Sylwia Huber,[1] Fethallah Benmansour,[1] Xing Chen,[1] Roberto Villaseñor,[1] Annamaria Braendli-Baiocco,[1] Matthias Festag,[1] Andreas Maunz,[1] Thomas Singer,[1] Franz Schuler,[1] and Adrian B. Roth[1]

[1]Roche Pharma Research and Early Development, Roche Innovation Center Basel, Basel 4070, Switzerland; [2]Roche Pharma Research and Early Development, Roche Innovation Center Copenhagen, Hørsholm 2970, Denmark

**Antisense oligonucleotide (AON) therapeutics offer new avenues to pursue clinically relevant targets inaccessible with other technologies. Advances in improving AON affinity and stability by incorporation of high affinity nucleotides, such as locked nucleic acids (LNA), have sometimes been stifled by safety liabilities related to their accumulation in the kidney tubule. In an attempt to predict and understand the mechanisms of LNA-AON-induced renal tubular toxicity, we established human cell models that recapitulate in vivo behavior of pre-clinically and clinically unfavorable LNA-AON drug candidates. We identified elevation of extracellular epidermal growth factor (EGF) as a robust and sensitive in vitro biomarker of LNA-AON-induced cytotoxicity in human kidney tubule epithelial cells. We report the time-dependent negative regulation of EGF uptake and EGF receptor (EGFR) signaling by toxic but not innocuous LNA-AONs and revealed the importance of EGFR signaling in LNA-AON-mediated decrease in cellular activity. The robust EGF-based in vitro safety profiling of LNA-AON drug candidates presented here, together with a better understanding of the underlying molecular mechanisms, constitutes a significant step toward developing safer antisense therapeutics.**

## INTRODUCTION

Current generation therapeutic antisense oligonucleotides (AONs) are single-stranded oligomers of synthetic nucleotides designed to hybridize to nucleic acids according to Watson-Crick base pairing.[1] To improve drug-like properties, including protein binding, their internucleotide links are generally phosphorothioated. Part of the nucleosides can also bear modifications such as locked nucleic acids (LNA), 2′-*O*-methoxyethyl (MOE), and 2′-*O*-ethyl (cEt), that further increase biostability and target affinity. One of the most affinity-enhancing sugar modifications is the locked nucleic acid (LNA). AONs with two chemically modified wings and a DNA gap in-between are known as gapmers. These are able to hybridize to a transcript and recruit ribonuclease H (RNaseH), resulting in degradation of the target.[2]

Accumulation in renal proximal tubules is a well-known component of the safety profile of AONs across chemical modifications.[3,4] Cell morphology changes observed include basophilic cytoplasmic granules or vacuoles in the proximal tubular epithelial cells shown to reflect accumulation of oligonucleotide in phagolysosomes.[2] Above a concentration threshold variable from molecule to molecule, degenerative/regenerative changes may be observed.[5,6] These findings typically consist of tubular degeneration with sloughing of individual cells into the lumen, tubular cell atrophy, and tubular regeneration/diffuse basophilia. Consistent with the long half-life of these molecules, toxicity generally takes weeks to develop.[7] Structural changes generally correlate with serum creatinine elevations, sometimes at late onset. Kidney injury biomarkers detectable in urine, such as kidney injury molecule 1 (KIM-1), could potentially detect tubulotoxicity during pre-clinical development although their value remains to be validated for AONs.

As of today, the mechanisms of AON-related tubulotoxicity are poorly understood and may differ across species. For a given AON compound, the risk is concentration-related. However, there are high accumulation compounds that are well tolerated and conversely, low accumulation compounds in the kidney cortex that are toxic. Cell uptake, intracellular trafficking, and localization may differ across AON molecules and explain some of the observed diversity. Similar to putative mechanisms in the liver, AONs may interact with critical intracellular proteins to disrupt their function[8] or may hybridize to unintended transcripts with a detrimental impact on pathways involved with cell maintenance.[9,10] The lack of in vitro models that mimic the in vivo toxicity of AONs has considerably limited the mechanistic understanding of the effect of these compounds at a cellular level.

Received 21 August 2016; accepted 21 November 2016;
http://dx.doi.org/10.1016/j.omtn.2016.11.006.

**Correspondence:** Annie Moisan, PhD, Roche Innovation Center Basel, Grenzacherstrasse 124, Basel 4070, Switzerland.
**E-mail:** annie.moisan@roche.com

At least eight LNA-AONs have reached early development stage to-date. Some LNA-AONs exhibited acceptable safety profiles,[11] but others were limited by their toxicity, including renal toxicity. A well-known case of the latter was SPC5001, a PCSK9-targeting drug candidate for hypercholesterolemia.[12,13] In this example, a dose-related renal tubular toxicity in a clinical phase 1 study led to the termination of this program while the pre-clinical toxicity package, conducted in mice and non-human primates, had not detected a specific renal cause for concern. Five days after receiving the third weekly dose, one high-dose subject incurred clinical acute tubular necrosis in this trial and underwent kidney biopsy. Histopathology showed normal glomeruli, no interstitial involvement, but multifocal tubular necrosis.[12,13] Follow-up non-clinical investigations on this molecule revealed that the rat, at higher doses, would have detected this signal.[14] While short-term studies in rodents still bring value in late discovery on a limited number of leads, there is a high demand for in vitro assays of human relevance that could be used upstream to de-select AONs within short testing cycles and rapidly inform the design of new molecules with improved therapeutic window.

To this end, we established an in vitro assay using human primary proximal tubule epithelial cells (PTEC) that fully recapitulates, for the first time, the in vivo nephrotoxicity of a panel of AONs, including the clinically-annotated SPC5001. We identified extracellular epidermal growth factor (EGF) as a robust in vitro predictor of LNA-AON-mediated tubulotoxicity and linked its elevation to a time-dependent reduced uptake by the EGF receptor (EGFR). We further explored the regulation of EGFR signaling by LNA-AONs and uncovered the down-modulation of *EGFR* activity and downstream transcriptional signature by tubulotoxic AONs.

## RESULTS

### Establishment of a Human Renal Cell Model that Recapitulates the In Vivo Liabilities of AONs

We first focused on establishing a human cell model capable of capturing the tubulotoxicity of a PCSK9-targeting LNA-AON drug (SPC5001, herein AON-B) terminated in clinical phase I after the occurrence of overt tubulotoxicity in a healthy volunteer.[12,13] Because AON-B triggered subtle toxicity signals in the remainder of the clinical cohort and is considered moderately toxic in short-term rat studies, we selected for comparison a second PCSK9-targeting LNA-AON (AON-C) classified as severely nephrotoxic in rats. A scramble LNA-AON (herein AON-A) was shown to have an innocuous profile in rodent studies and was thus selected as a negative control (Figure 1A). Rat kidney histopathology findings for these three test AONs are summarized in Table 1, and examples of renal histological alterations induced by AON-B and AON-C are shown in Figures 1B and S1. Because AON accumulation in the kidney occurs mainly in the proximal tubule, we tested the responsiveness of human primary and telomerase reverse transcriptase 1 (TERT1)-immortalized PTEC to selected AONs. To mimic the physiological exposure of renal tubules to circulating naked AONs (i.e., without assistance of delivery technology), non-dividing confluent monolayers of PTEC and PTEC-TERT1 were exposed to an aqueous solution of AON (herein referred to as gymnotic delivery). AON were administered at concentrations of 1 to 100 μM, which approximate the renal concentrations of AON detected in cynomolgus monkeys after repeated dosing[5] (see the Materials and Methods). Medium with AONs was changed every 3 days and intracellular ATP was measured as an indication of cell metabolism and viability (Figure 1C). In accordance with the relatively late onset renal failure in human and histopathological manifestations in rodents, our preliminary analyses showed that AON B-mediated effects on intracellular ATP in PTEC-TERT1 became evident after several days of treatment (Figure S2). The ATP readout was therefore performed at day 9 throughout this study (Figure 1C). Using this cell model and experimental design, the toxicity grade of AONs A, B, and C could be accurately recapitulated, i.e., AON-C was more cytotoxic than AON-B, and AON-A appeared innocuous (Figure 1D). Measurement of the levels of targeted and untargeted mRNAs, namely *PCSK9* and *MALAT1*, respectively, confirmed efficient and specific target knockdown by both PCSK9-targeting AONs after 3 days of exposure (Figure 1E). These findings (1) rule out that lower cytotoxicity of AON-B compared to AON-C is a consequence of inferior pharmacology, (2) demonstrate that gymnotically delivered AONs enter the "productive compartment"[15] of PTEC (i.e., reach their RNA target), and (3) reveal that efficacy largely precedes cytotoxicity as measured by intracellular ATP. Thus, the mode of toxicity described here seemingly requires time-dependent intracellular accumulation of AON or accumulation of AON-induced cellular and molecular alterations.

Cell morphological changes induced by AON-B appeared different than those by AON-C under bright field microscopy (Figure 1F, upper panels). AON B-treated PTEC-TERT1 formed irregular domes and vacuoles whereas AON-C-treated PTEC-TERT1 adopted a flattened and stable appearance. Cytoskeleton and nuclei staining indicated that the decrease in cellular ATP induced by AONs B and C is not associated with a significant decrease in cell numbers (Figure 1F, lower panels). Quantification of cellular protease activity in cell supernatant suggested that disruption of cell membrane integrity occurred after treatment with AON-B but not AON-A nor C (Figure 1G). Finally, no sign of AON-induced caspase activation was detected in contrast to significant activation by the control tubulotoxicant staurosporine, suggesting that none of the three test AONs triggered apoptosis in the assay conditions (Figure 1H). Intriguingly, except for reducing intracellular ATP, the severely toxic AON-C appeared inert in the cellular assays described in Figure 1. Altogether, these data illustrate the diverse nature of AON-induced toxicities and the challenge of identifying a universal, predictive molecular marker.

### Identification of Extracellular EGF as an In Vitro Marker of AON-Induced Tubulotoxicity

Because intracellular ATP as a readout for AON safety screening requires a long (9 days) exposure period and cannot be translated into a practical molecular biomarker in the clinic, we searched for soluble factors present in the cell supernatant that are elevated after AON treatment in accordance with the severity of in vivo liability and prior to ATP decline. We used a multiplex ELISA technology to quantify

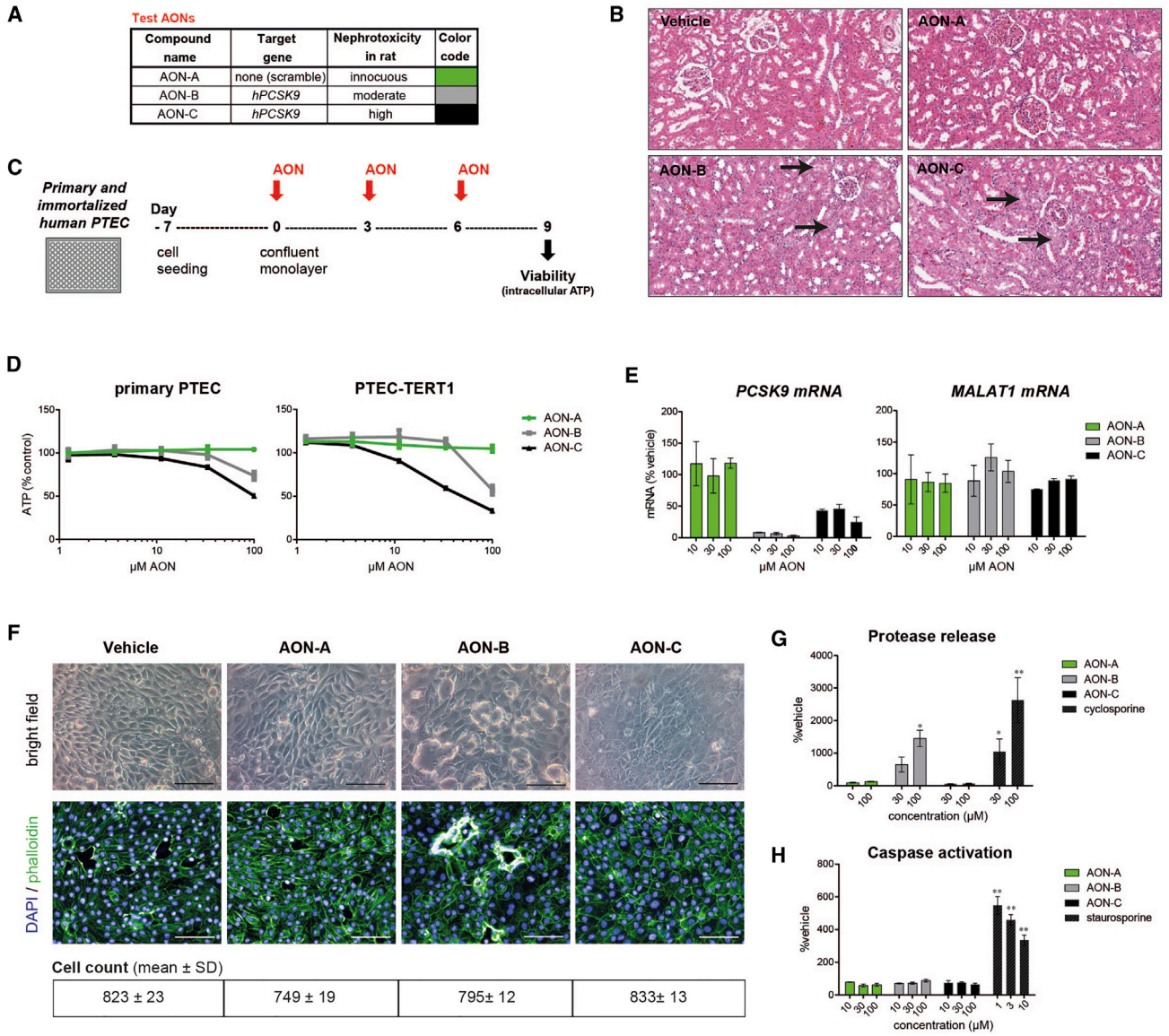


**Figure 1. In Vivo Tubulotoxicity of Test AONs Is Recapitulated in Human PTEC Models**

(A) Test AONs and their respective targets and in vivo toxicity score. (B) Histological evaluation of rat kidney. Arrows indicate examples of areas with tubular degeneration/regeneration in animals treated with AONs B and C. H&E, 20× magnification. Representative of n = 4 animals per group. (C) Schematic representation of assay design for AON safety profiling in PTEC. (D) Measurement of intracellular ATP showing dose-dependent negative effect of AON-B and AON-C on cell viability in primary PTEC and immortalized PTEC-TERT1. (E) Gene expression analysis showing efficient gene knockdown of *PCSK9*, but not *MALAT1,* by AON-B and AON-C in PTEC-TERT1 after 3 days of exposure. (F) Upper panels: bright field images showing different morphological alteration induced by 7 days of exposure to AON-B and AON-C in PTEC-TERT1. Lower panels: confocal images of nuclear (DAPI, blue) and cytoskeleton staining (phalloidin, green) of PTEC-TERT1 showing similar cell number for all conditions. Cell count was determined by counting the number of nuclei in five fields per condition and shown as mean and SD of three independent experiments. Scale bars, 50 µm. (G) Measurement of extracellular protease activity revealing signs of cell death in PTEC-TERT1 treated with AON-B. Cyclosporine was used as a positive control. (H) Measurement of caspase 3/7 activity in PTEC-TERT1 showing that none of the tested AON-induced apoptosis. Staurosporine was used as a positive control. Data in (D), (E), (G), and (H) represent means and SD (n = 3). *$p < 0.005$ and **$p < 0.0001$, ANOVA with Dunnett's multiple comparisons test.

the concentrations of 42 cytokines, chemokines, growth factors, and kidney injury biomarkers including KIM-1 (see the Materials and Methods for a complete list) in the supernatant of primary and immortalized PTEC treated with AONs A, B or C for 3 and 6 days (Figure 2A). Of the 42 tested proteins, only EGF was elevated in correlation with the degree of AON toxicity in a concentration-dependent manner in both primary and immortalized PTEC at days 3 and 6 (Figure 2B, upper panel). Fluctuations of cytokine and chemokine levels

**Table 1. Test AONs and Summary of Kidney Toxicity Assessed in 2-Week Rat Study at 40 mg/kg/week**

| ID | Target | Kidney Weight (%) | Urine Protein[a] | KIM-1 (Urine)[a] | Kidney De/Regeneration | Relative Tubulotoxicity Grade | Relative Toxicity Grade for In Vitro Study |
|---|---|---|---|---|---|---|---|
| A | Scramble | <+10 | 1.4 | 2.6 | – | low (no findings) | innocuous |
| B | *PCSK9* | <+10/10–20 | 1.9/4.2 | 9.7/92 | ++ to +++ | medium/medium | medium |
| C | *PCSK9* | +10–20/20–30 | 1.3/2.2 | 188/302 | ++ to ++++ | high/high | high |
| D | *PCSK9* | <+10 | 1.0/1.4 | 1.3/5.9 | + to ++ | low/low | low |
| E | *MYD88* | <+10 | 1.8 | 9.5 | ++ to +++ | medium/medium | medium |

Male rats were dosed at 40 mg/kg subcutaneously on days 1 and 8, before sacrifice on day 15; n = 8 (some of the compounds were tested twice in the same type of study, whenever values differ those are presented as follows: "value A/value B".
[a]Fold change from saline at sacrifice.

that were not correlated with the degree of AON toxicity were exemplified by interleukin 6 (IL-6), interleukin 8 (IL-8), and monocyte chemotactic protein-1 (MCP-1) (Figure S3). Supernatant concentrations of the PTEC-specific kidney injury biomarker KIM-1 were reduced after 6 days of treatment with high concentrations of both toxic AONs and slightly but reproducibly elevated with innocuous AON-A (Figure 2B, lower panel). It is worth noting that KIM-1 levels in supernatants of untreated human primary and TERT1-immortalized PTECs are readily elevated in conventional culture conditions in comparison to the barely detectable *KIM-1* expression of healthy renal cortex.[16,17] To verify that elevated EGF is a general marker of AON-induced cytotoxicity and does not depend on PCSK9 knockdown, a validation test was performed with two additional tool AONs previously profiled in comparable rat studies: AON-D, a mildly toxic AON and the best tolerated of a PCSK9 series, and MYD88-E, a *MYD88*-targeting AON reported to cause kidney pathologies (Figure 2C; Table 1). A gene expression analysis was performed to confirm that PCSK9 mRNA is reduced in cells exposed to AON-D but not to the *MYD88*-targeting AON-E (Figure S4). Immortalized PTEC (herein PTEC-TERT1) were preferred to primary PTEC to pursue validation and characterization of EGF because of their replicative potential and stable phenotype, providing a more robust cellular model for safety screens. Similar to AON-B and AON-C, intracellular ATP was reduced and extracellular EGF was elevated after exposure to AON-E in a concentration-dependent manner (Figures 2C and 2D). Accumulation of EGF after exposure to toxic AONs was observed as early as day 3 and was more pronounced at days 6 and 9 despite medium change every 3 days, suggesting that the underlying cellular mechanism is exacerbated over time (Figure 2D). The slight EGF elevation observed at day 9 in AON-D-treated PTEC-TERT1 is consistent with the variable degree of histopathological findings reported in a subset of AON-D-treated rats (Figure S5) confirming the sensitivity of the in vitro assay. As observed above (Figure 2B), KIM-1 profile was variable and not consistently associated with cytotoxicity: subtle elevations were noticeable for AON-A and AON-D at days 6 and 9 and for low concentration of AON-E at day 9 whereas a marked decrease was measured for the severely toxic AON-C (Figure 2D, lower panel). Hence, KIM-1 upregulation appeared to reflect an early stress response to AONs that is no longer perceptible upon aggravated cellular or molecular dysfunction.

Altogether the data showed that measurement of extracellular EGF offers a promising assay to predict AON liabilities and prompted us to investigate the nature and significance of EGF accumulation in response to AON treatment.

### Impairment of EGF Uptake in Toxic AON-Treated Cells

Mechanistic investigations of EGF as a biomarker of AON-induced toxicity should take into account that (1) the medium of PTEC is supplemented with human EGF as a growth factor for the cells, and (2) proximal tubule cells are known to express the EGF receptor (EGFR) and respond to EGF.[18] More importantly, in vivo, EGF is produced by distal but not proximal tubules.[18] Therefore, the elevation of EGF in the supernatant of PTEC-TERT1 is most likely a result of dysfunctional uptake by EGFR rather than a stimulated production and secretion of EGF. We verified this hypothesis by confirming that PTEC-TERT1 efficiently deplete EGF from the medium within 72 hr (Figure 3A), express EGFR, and do not express detectable level of EGF even after exposure to AONs (Figure 3B). In addition, we compared the EGF profile of AON-treated PTEC-TERT1 in the presence and absence of extracellular EGF in the medium and observed that accumulation of soluble EGF occurred only when the medium was supplemented with EGF (Figure 3C). To visualize the capacity of AON-treated cells to internalize extracellular EGF, PTEC-TERT1 were exposed to AONs for 6 days, incubated overnight without EGF, and incubated 10 min at 37°C with a fluorescently labeled EGF (EGF-488) in AON-free medium (scheme Figure 3D). EGF uptake and intracellular accumulation was visible in the form of green foci in vehicle-treated cells and was fully blocked by simultaneous incubation with cetuximab, a monoclonal antibody that blocks EGF binding to EGFR[19] (Figure 3D, upper panels). AON-A-treated cells normally accumulated EGF-488, whereas pre-exposure to toxic AON-D, AON-B, AON-C, and AON-E significantly reduced the number of EGF-488 foci (Figure 3D, lower panels; see Figure S6 for quantification). The decreased number of intracellular EGF foci together with the accumulation of EGF in the medium suggest that EGF uptake is dysfunctional in toxic AON-treated PTEC-TERT1 cells.

To determine whether AON-mediated alterations in EGF transport are restricted to a renal epithelial cell model, we replaced PTEC-TERT1 with human primary hepatocytes, a cell model that is

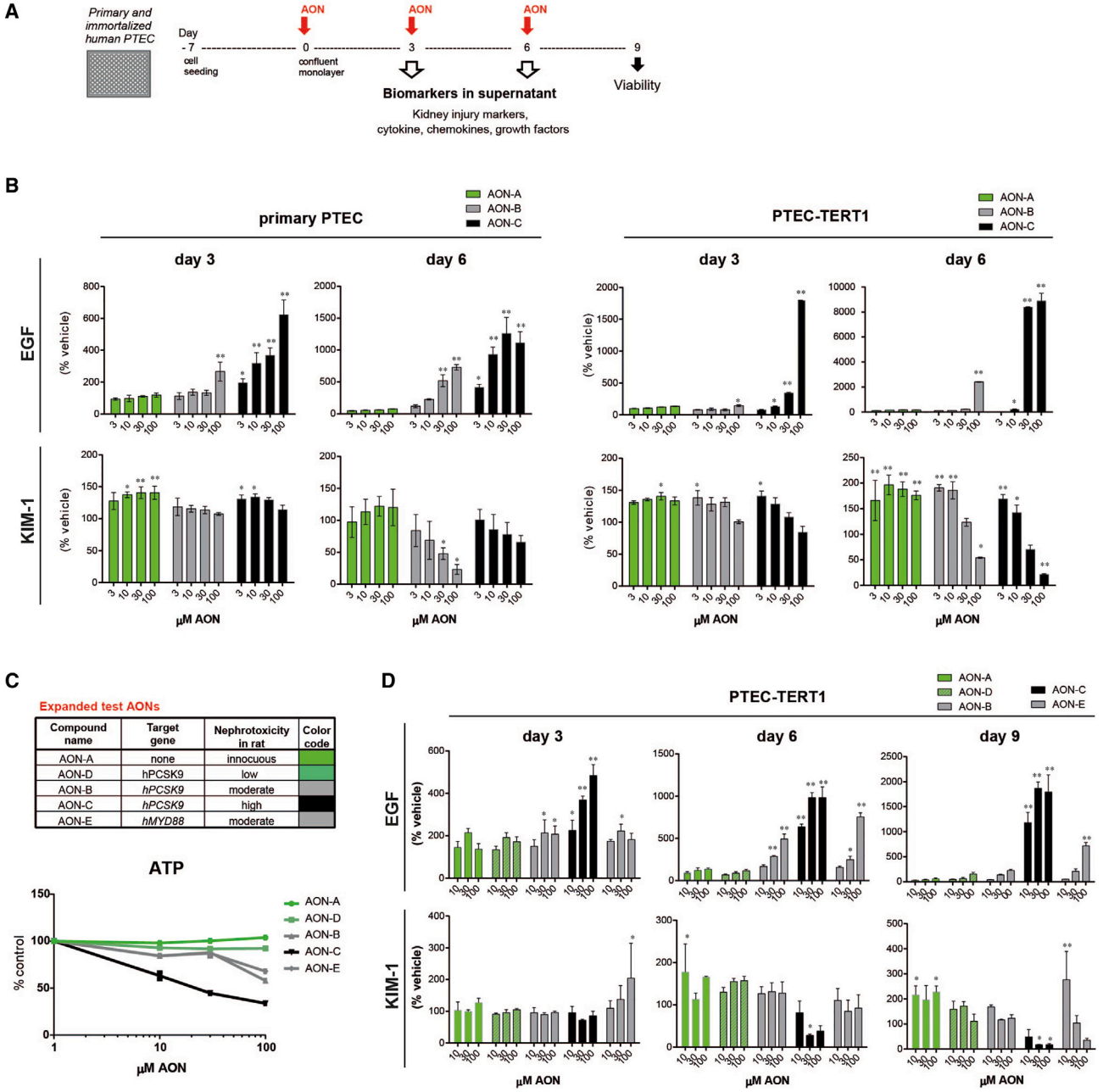


**Figure 2. Extracellular EGF Is a Robust Marker of AON-Induced Tubulotoxicity In Vitro**

(A) Schematic representation of assay design for identification of soluble markers predictive of AON-mediated tubulotoxicity. (B) Multiplex-ELISA analysis of AON-treated PTEC supernatants showing that EGF, but not KIM-1, is increased in a time- and dose-response manner in toxic AON-treated cells. (C) Upper panel: expanded test AONs and their respective targets and relative in vivo toxicity score. Lower panel: measurement of intracellular ATP showing dose-dependent negative effect of AONs B, C, and E on cell viability in PTEC-TERT1. (D) Duplex ELISA analysis of AON-treated PTEC supernatants showing that increased levels of EGF, but not KIM-1, correlate with in vivo toxicity profile. Data in (B)–(D) represent means and SD (n = 3). *p < 0.01 and **p < 0.0001, two-way ANOVA with Dunnett's multiple comparisons test.

competent for gymnotic uptake of AONs,[20] expresses EGFR but is not dependent on EGF for in vitro proliferation and survival (Figure S7). Human hepatocytes cultivated and seeded in a conventional EGF-free medium were exposed to safe and tubulotoxic AONs along with 10 ng/mL of EGF. Intracellular ATP and extracellular EGF were measured concomitantly after 3 days of AON exposure. AON-B and AON-C showed significantly elevated EGF levels whereas AONs D and E had minimal changes in EGF (Figure 3E). AON-C

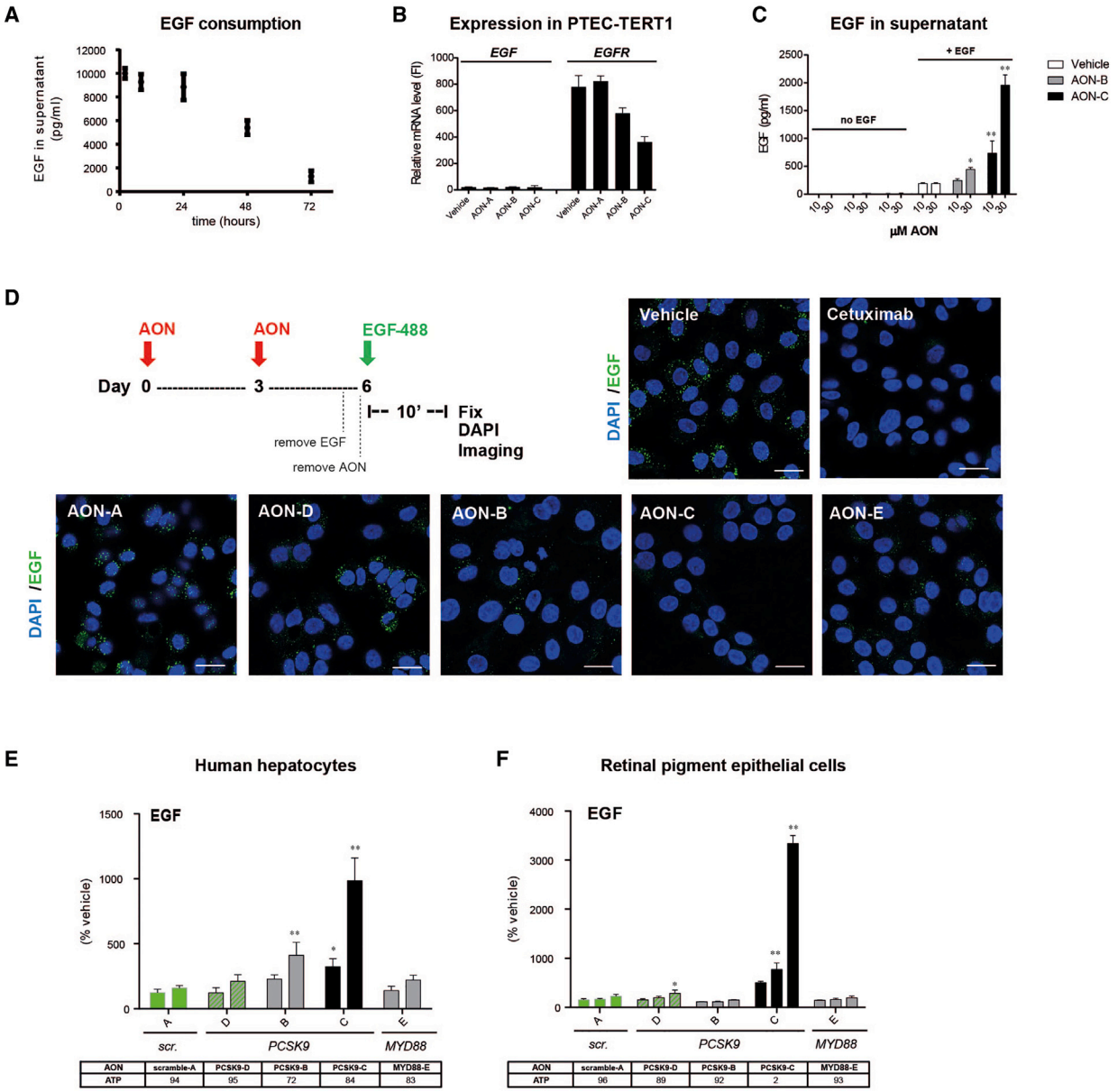


**Figure 3. Exposure to Toxic AONs Impair EGF Uptake by EGFR**

(A) Consumption of extracellular EGF by PTEC-TERT1 over time. (B) Gene expression analysis showing that EGFR, but not EGF, is expressed in vehicle and AON-treated PTEC-TERT1. (C) Measurement of EGF in the supernatant of AON-treated PTEC-TERT1 showing that addition of EGF in the cell medium is necessary to use EGF as an in vitro biomarker. (D) An EGF uptake assay was performed by subjecting AON-treated PTEC-TERT1 (6 days) to EGF-488 for 10 min followed by nuclear staining and confocal imaging. Accumulation of EGF-488 (green dots) was fully blocked by cetuximab and reduced in cells treated with AONs D, B, C, and E compared to vehicle. Scale bars, 20 μm. For data quantification, see Figure S5. (E) Measurement of EGF in the supernatant of human hepatocytes treated with 10 and 100 μM of AONs for 3 days. Intracellular ATP value is shown for 100 μM of AONs as percentage of vehicle control. scr., scramble. (F) Measurement of EGF in the supernatant of retinal pigment epithelial cells treated with 10, 30, and 100 μM of AONs for 7 days. Intracellular ATP value is shown for 100 μM of AONs as percentage of vehicle control. Data in (A)–(C), (E), and (F) represent means and SD (n = 3). *p < 0.01 and **p < 0.0001, two-way ANOVA with Sidak's (C and E) or Dunnett's (F) multiple comparisons test.

did not lead to a substantial reduction in intracellular ATP in human hepatocytes despite strong EGF elevation, thus uncoupling the two readouts and implying that reduced EGF uptake is not solely caused by a general cellular deterioration. In addition, we exposed the ARPE-19 retinal pigment epithelial cell line to AONs in cell medium supplemented with EGF. We observed an accumulation of EGF in the supernatant of AON-C-treated ARPE-19 associated with a decrease in intracellular ATP (Figure 3F). Interestingly, ARPE-19

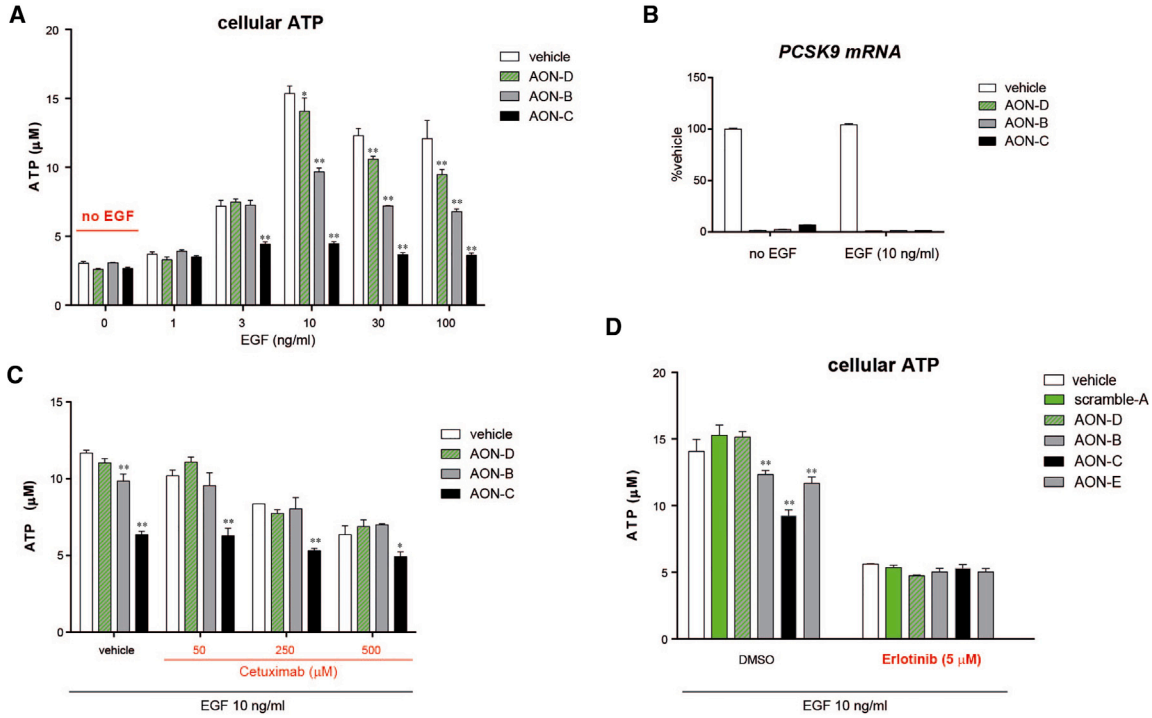


**Figure 4. Toxic AONs Block EGF-Induced and EGFR-Dependent Cellular Activity**

(A) Measurement of intracellular ATP in confluent PETC-TERT1 showing that the positive effect of EGF on cellular activity is blocked by AONs D, B, and C. (B) Gene expression analysis confirming efficient target reduction by AON-D, AON-B, and AON-C independent of EGF. (C and D) Measurement of intracellular ATP in PETC-TERT1 showing that inhibition of EGFR signaling using cetuximab (C) or erlotinib (E) decreases cellular energy and reduces or masks the effect of toxic AONs. AONs were applied at a final concentration of 100 µM in (A)–(D). Data in (A)–(D) represent means and SD (n = 3). *$p < 0.01$ and **$p < 0.0001$, ANOVA with Dunnett's multiple comparisons comparing AONs to vehicle under the same concentration of EGF (A), cetuximab (C), or erlotinib (D).

did not show signs of cytotoxicity in response to AON-B and AON-E, thus highlighting the importance of choosing the most appropriate and responsive cell model to fully capture the toxicity potential of AONs with correlation to histopathology findings.

### Blockage of EGF-Induced and EGFR-Dependent Cellular Activity by Toxic AONs

Following the finding that tubulotoxic AONs impair EGF uptake, we assessed whether tubulotoxicity is correlated with the amount of extracellular EGF in the medium. PTEC-TERT1 were grown until confluence in regular EGF-containing medium (10 ng/mL) and measurements of intracellular ATP and extracellular EGF accumulation were performed after simultaneous incubation with AON along with 0, 1, 3, 10, 30, or 100 ng/mL of EGF. This experiment showed that regulation of intracellular ATP levels in confluent, non-dividing PTEC-TERT1 is dependent on EGF concentration (Figure 4A). Remarkably, the toxicity profile of AONs D, B, and C was no longer observed at 0 and 1 ng/mL of EGF, and noticeable differences between innocuous and toxic AONs required 10 ng/mL or higher concentrations of EGF (Figure 4A). Importantly, AON target reduction was not affected by the presence or absence of EGF (Figure 4B). These data suggest that toxic AONs may block EGF-dependent cellular energy production. To further investigate this hypothesis, we monitored the effect of AONs after inhibition of EGFR signaling with Cetuximab. Similar to toxic AONs, cetuximab alone reduced EGF-induced intracellular ATP (Figure 4C). The combination of AONs and cetuximab had little synergistic or additional effects on ATP levels, suggestive of a common mode of action via inhibition of EGFR signaling. To corroborate these observations, the toxicity profile of AONs was assessed in the presence of erlotinib, a small molecule inhibitor of EGFR kinase activity. In agreement with our hypothesis, the ATP profile of innocuous and toxic AONs was undistinguishable in EGFR-inactivated cells via erlotinib (Figure 4D).

Altogether, these data provide strong evidence that inhibition of EGFR signaling may be a central mechanism of AON-induced cytotoxicity in PTEC models.

### Modulation of EGFR Trafficking and Signaling by Toxic AONs

AONs are poly-anionic molecules capable of binding to cell surface proteins and growth factors,[21,22] and it is conceivable that direct AON/EGF or AON/EGFR interactions initiate a negative regulation of EGFR that progressively leads to weakening of EGFR activity and decreased cellular activity. We assessed the direct interactions of five selected AONs with EGF and the extracellular domain of EGFR, separately and in combination, using label-free surface

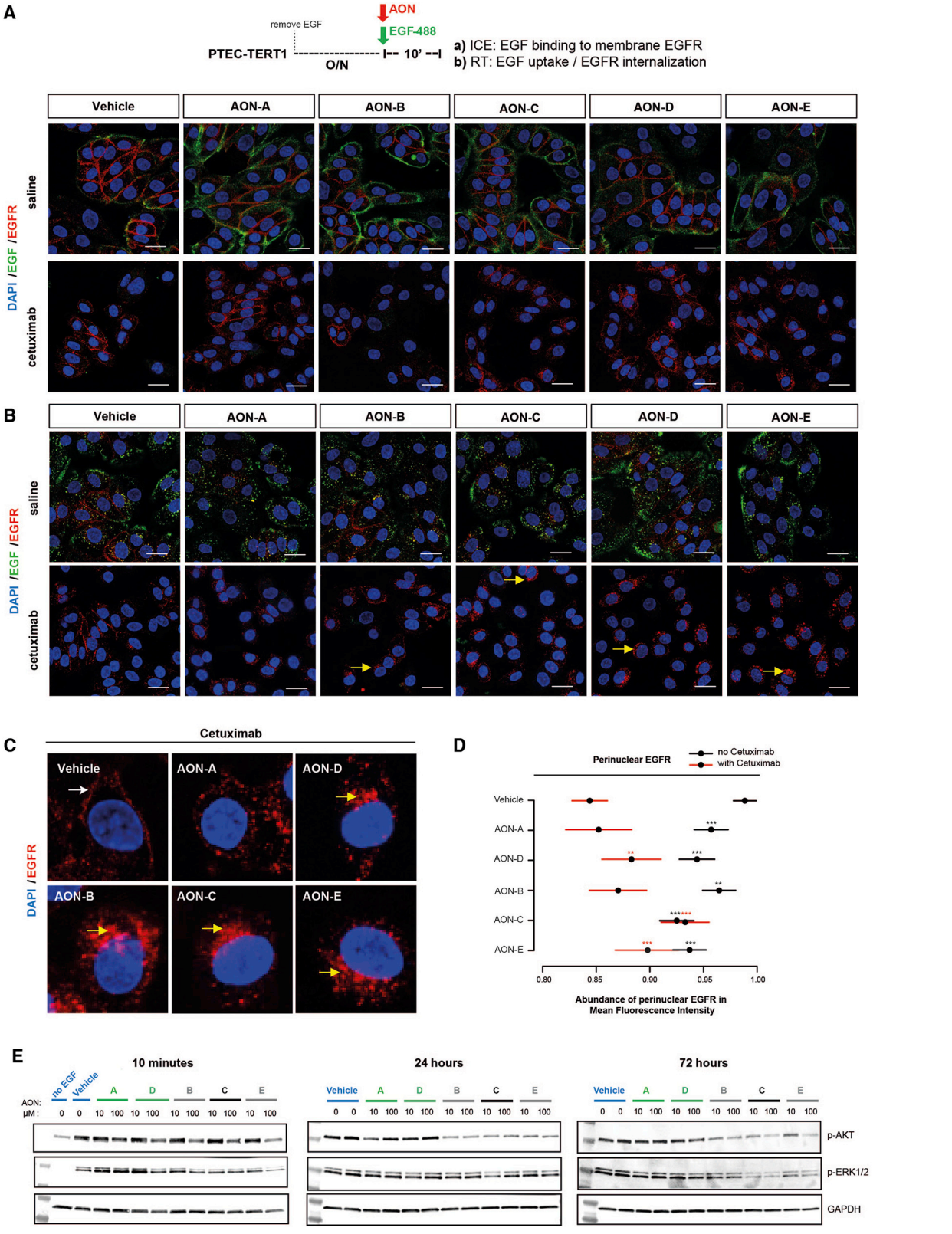


*(legend on next page)*

plasmon resonance (SPR). Despite robust interaction between EGF and EGFR, no direct AON/protein interaction could be detected between any of the five tested AONs and EGF or EGFR (Figure S8). Moreover, the data suggest that AONs did not interfere with the binding of EGF to EGFR in a cell-free system. We therefore used a fluorescence-based cellular assay that preserves the native conformation of membrane-bound receptors to visualize the binding of EGF to EGFR and the internalization of the EGF/EGFR complex. Briefly, EGF-starved PTEC-TERT1 were exposed to innocuous and toxic AONs in the presence of a fluorescently labeled EGF (EGF-488) for 10 min on ice to prevent internalization from the plasma membrane. PTEC-TERT1 cells were fixed and EGFR was visualized by immunodetection. Binding of EGF-488 to the cellular membrane was evident for all conditions including PTEC-TERT1 exposed to toxic AONs (Figure 5A, upper panels). Addition of cetuximab completely abolished the binding of EGF-488 to the cell membrane and thereby confirmed the specific and effective binding of EGF-488 to EGFR for all treatments (Figure 5A, lower panels). Next, to visualize the internalization of EGF/EGFR, PTEC-TERT1 were incubated with EGF-488 at 37°C. Cellular uptake of EGF-488 was evident in both the vehicle and AON-exposed PTEC-TERT1 (Figure 5B, upper panels) and exclusively mediated by EGFR because the addition of cetuximab completely abolished the internalization of EGF-488 in all conditions (Figure 5B, lower panels). In agreement with this image-based assay, quantification by flow cytometry showed similar EGF-488 uptake by PTEC-TERT1 in the presence of innocuous and toxic AONs (Figure S9). We conclude that these AONs do not significantly interfere with EGF binding to EGFR and that simultaneous acute incubation with EGF and AONs does not directly block EGF uptake. Intriguingly, in cells exposed to AONs D, B, C, and E, EGFR was internalized in the presence of cetuximab and was not associated with any detectable EGF-488 signal (Figures 5B and 5C, arrows). In all conditions except vehicle and AON-A, a subpopulation of cells showed a perinuclear distribution of EGFR (Figure 5C, arrows). We developed a method to quantify the presence of EGFR foci located at a fixed distance from the nucleus (perinuclear EGFR) and determined the mean intensity of perinuclear EGFR per cell. In vehicle-treated cells, co-incubation with EGF and cetuximab maintained EGFR at the cell membrane (Figure 5C, arrow), which is translated as a left shift on the quantification graph of perinuclear EGFR (Figure 5D). Incubation with toxic AONs significantly disrupted the cetuximab-dependent distribution of EGFR between the plasma membrane and the perinuclear compartment: the amount of EGFR at the cell membrane was diminished and accumulation of perinuclear EGFR was increased (Figures 5D and S10). The molecular nature of perinuclear EGFR foci caused by toxic AONs, unveiled here by the use of cetuximab, remains to be elucidated in future studies. Nevertheless, these observations suggest that toxic AONs induce ligand-independent internalization of EGFR.

Next, the acute effect of AONs on EGFR kinase activity was determined by immunoblot analysis of AKT and ERK1/2 phosphorylation. PTEC-TERT1 were exposed to EGF and AONs and harvested after 10 min of incubation. Downregulation of phosphorylation of AKT by toxic AON-C and E was readily apparent after 10 min of exposure (Figures 5E, left panel, and S11). The effects of toxic AON-B, AON-C, and AON-E on phosphorylation of AKT and ERK1/2 were more pronounced after 24 and 72 hr of AON exposure (Figures 5E, middle and right panels, and S11), likely reflecting a reduced steady-state level of EGFR signaling in toxic AON-exposed cells. Such reduction is not caused by a general toxicity effect, since the nephrotoxicant cyclosporine A (CysA) did not reduce the phosphorylation level of AKT and ERK1/2 relative to the GAPDH protein loading control (Figure S12). The effect of AON-D on EGFR activity could not be detected by measurement of AKT and ERK1/2 phosphorylation level, hypothetically due to compensatory signals or feedback mechanisms, which would also explain the variable profile of AON-D across in vivo studies in rodents (Table 1; Figure S5).

Together, these results reveal acute effects of toxic AONs on EGFR cellular distribution and kinase activity and suggest that reduced EGF uptake in toxic AON-exposed PTEC-TERT1 occurs progressively as a consequence of dysfunctional EGFR trafficking and signaling.

### Impairment of an EGF Transcriptional Signature by Toxic AONs

In order to further investigate the effects of AONs on EGF-dependent responses at early time points, we used molecular phenotyping, a recently introduced technology to infer human pathway activities by quantifying expression of pathway-reporter genes with next-generation sequencing.[23] PTEC-TERT1 were treated with innocuous and toxic AONs in the presence or absence of EGF for 6 hr, total RNA was isolated and pathway reporter genes were quantified based on sequencing of predefined amplicons.[24] To derive a list of genes that are modulated by extracellular EGF in PTEC-TERT1 (EGF signature herein), we compared expression profiles of vehicle-treated cells with and without EGF and identified 66 genes that are consistently

**Figure 5. EGFR Trafficking and Signaling Are Altered by Toxic AONs Acutely**

(A–D) Visualization of EGF binding (A) and internalization (B and C) by EGFR: PTEC-TERT1 were exposed to EGF-488 along with vehicle or 100 μM of AONs for 10 min on ice (A) or at 37°C (B and C). Cetuximab was added 5 min prior to EGF-488 and AONs where indicated to block EGF binding sites. EGFR was revealed by immunofluorescence and nuclei by DAPI staining. No significant differences in EGF uptake were observed between vehicle and AONs. Scale bars, 20 μm. White arrow, cytoplasmic membrane accumulation of EGFR in the presence of cetuximab in control cells. Yellow arrow, perinuclear accumulation of EGFR in the presence of cetuximab and toxic AONs. (D) Quantification of the abundance of perinuclear EGFR under cetuximab condition. Data are presented as mean fluorescence intensity in a defined perinuclear area (log transformed). *$p < 0.05$, **$p < 0.01$, ***$p < 0.001$, least-squares model, n = 1,117. See the Materials and Methods for details on image processing and statistical analysis. (E) Immunoblot analysis showing that phosphorylation of AKT and ERK is slightly reduced by short exposure of PTEC-TERT1 to AONs D, B, C, and D (10 min) and more significantly reduced after 24 and 72 hr of AON exposure. Representative of n = 2 per time point. Quantification is provided in Figure S10 and uncropped gels are provided in Figure S13.

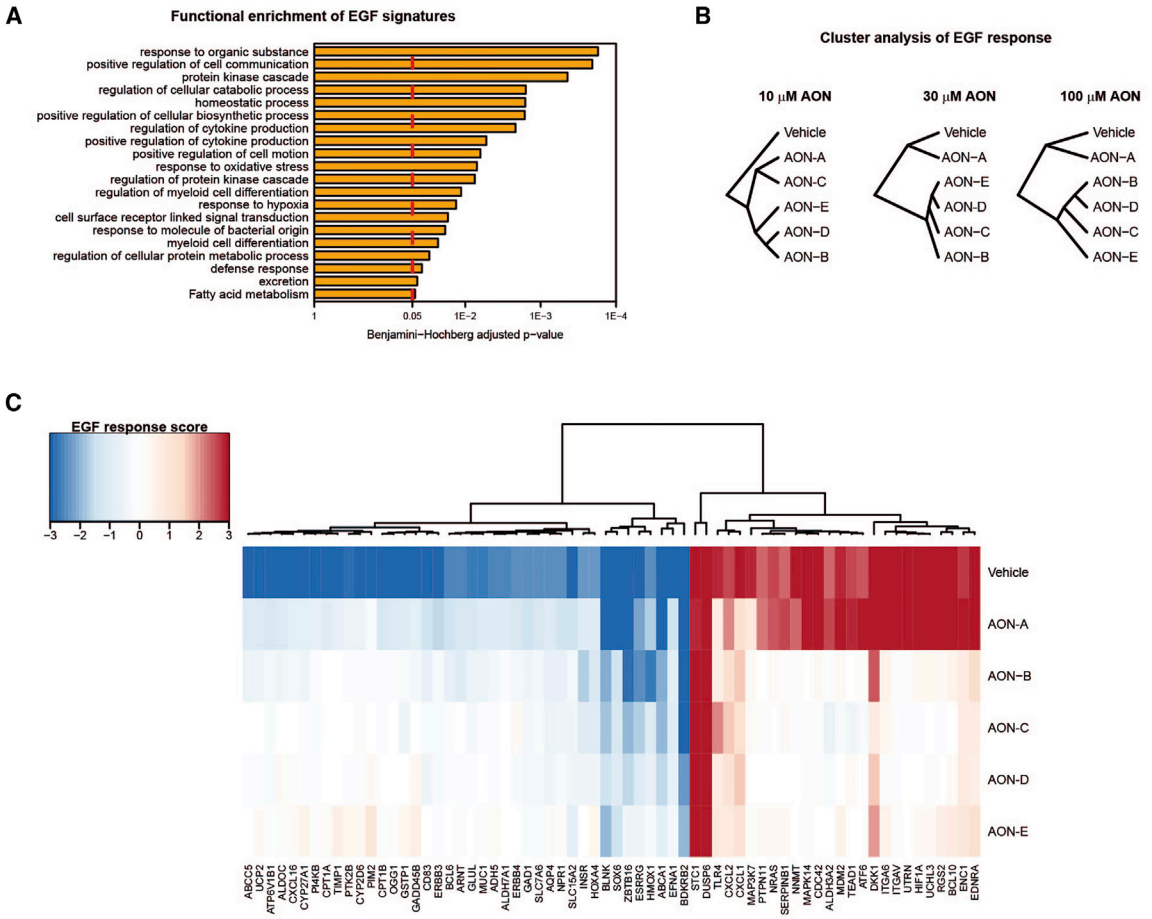


**Figure 6. An EGF-Induced Transcriptional Signature Is Impaired by Toxic AONs in PTEC-TERT1**

(A) Functional enrichment analysis of EGF-modulated genes in PTEC-TERT1 after 6 hr of EGF exposure. The most significantly enriched gene sets with the lowest adjusted p value are shown. Benjamini-Hochberg adjusted p value of Fisher's exact test no larger than 0.05. (B) Cluster analysis of changes of the EGF signature revealing that at 30 μM and 100 μM, AON-A cluster with the vehicle control while toxic AONs diverge from control. (C) Heatmap visualization of the EGF signature at 6 hr showing that 30 μM of toxic AONs abolished the EGF signature of both positive and negative EGF-dependent modulation.

positively or negatively modulated by EGF. We performed functional enrichment analysis of EGF signatures and observed that genes induced by EGF have versatile biological functions such as signal transduction, cytokine production, response to oxidative stress and hypoxia, defense response, and fatty acid metabolism (Figure 6A). It is worth mentioning that no gene set directly associated with cell cycle or apoptosis passed the significance threshold. The signature allowed us to interrogate whether AON treatments impaired EGF signaling. Cluster analysis of EGF-induced changes of the signature revealed that treatment with toxic AONs altered the downstream expression output of EGF signaling as early as 6 hr compared with vehicle control. At 30 and 100 μM, the innocuous AON-A and vehicle clustered together while AON-B, AON-C, AON-D, and AON-E displayed substantially different profiles (Figure 6B). Next, we used heatmap visualization of expression changes to compare the effects of AONs on the EGF signature after 6 hr of exposure at 30 μM. The vehicle control highlights positively and negatively regulated genes in the EGF versus no-EGF condition (Figure 6C). The EGF-induced signature (red signals) is preserved in AON A-treated cells consistent with the innocuous profile observed in vitro and in vivo under our experimental conditions. Interestingly, several genes strongly down-regulated by the presence of EGF (blue signals) were less modulated in the presence of AON-A, suggesting a general effect of AONs that is not deleterious for normal cellular function. Remarkably, AON-B, AON-C, AON-D, and AON-E almost abolished the EGF signature of both positive and negative EGF-dependent modulation (Figure 6C). Interestingly, all four potentially toxic AONs showed a similar profile in this analysis, including AON-D. Therefore, molecular phenotyping analysis of EGF-induced signature is a sensitive and powerful approach to detect the tubulotoxicity potential of AONs.

Overall, molecular phenotyping data revealed that only known toxic AONs inhibit EGF signaling as early as 6 hr after treatment, consistent with molecular and cellular analyses of EGFR signaling.

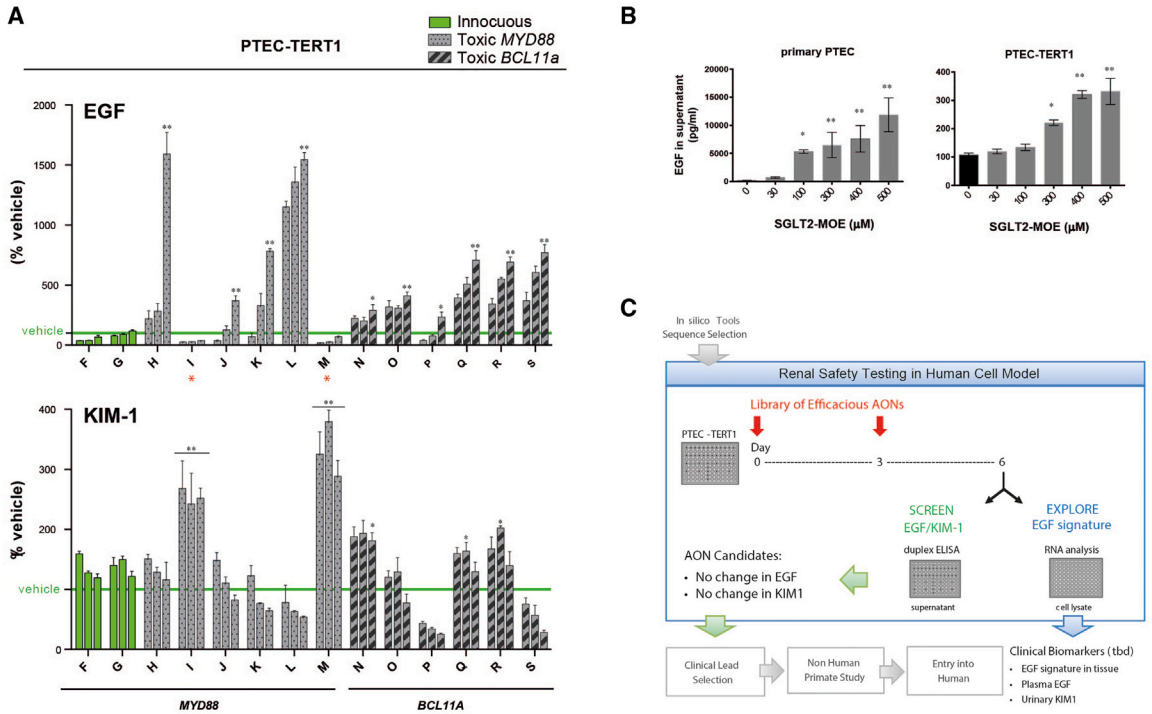


**Figure 7. Extracellular EGF Correlates with AON-Induced Adverse Effects across Pre-clinical AON Series**

(A) Duplex ELISA analysis of AON-treated PTEC-TERT1 supernatants showing that increased levels of EGF correlated with in vivo toxicity profile for all tested AONs except MYD88-I and MYD88-M (*). Conversely, highest increased of KIM-1 levels correlated with in vivo toxicity of MYD88-I and MYD88-M. AONs were applied at 10, 30, and 100 μM. Data represent means and SD (n = 3). *$p < 0.01$ and **$p < 0.0001$, ANOVA with Dunnett's multiple comparisons comparing AONs to vehicle. For figure clarity, p values of EGF are shown for 100 μM only. (B) Measurement of EGF in the supernatant of human primary and TERT1-immortalized PTEC treated for 6 days with up to 500 μM of a non-LNA AON containing the 2′-*O*-methoxyethyl (MOE) modification. Data represent means and SD (n = 3). *$p < 0.02$ and **$p < 0.0001$, ANOVA with Dunnett's multiple comparisons comparing AON to vehicle. (C) Implementation of the EGF assay in pre-clinical AON safety screen: a library of efficacious AONs is applied to a confluent monolayer of PTEC-TERT1 gymnotically (without delivery assistance). Measurement of EGF in the cell supernatant serves as a toxicity biomarker and KIM-1 is monitored alongside as a complementary readout. AONs for which extracellular EGF and KIM-1 remain unchanged are prioritized for animal studies. Exploring the EGF-induced transcriptional signature in vitro and in vivo may provide additional clinically translatable markers.

### Safety Assessment across Pre-clinical AON Series Using Extracellular EGF

To validate the use of EGF as a biomarker in discovery and pre-clinical kidney safety screens, we reviewed pre-clinical studies available to our group and selected an additional 12 LNA-AON compounds targeting *MYD88* or *BCL11A* with reported gross anatomical changes in mouse kidneys or histopathological findings in rat kidneys (Table S1). Two additional innocuous AONs were included as controls. For all 14 AONs, supernatant concentrations of EGF and KIM-1 at day 6 were measured and reported in percentage of vehicle control. Elevation of EGF in the supernatant of PTEC-TERT1 accurately matched the in vivo liabilities of 12 of the 14 AONs, a score superior to elevation of KIM-1 (only 3/14 at 100 μM) (Figure 7A). As observed previously for AON-B, AON-C, and AON-E (Figure 2D), increasing doses of toxic AONs J, K, L, O, P, and S lead to a decrease in KIM-1 level. Interestingly, elevated KIM-1 predicted the toxicity of MYD88-I and MYD88-M, the only two AONs that the EGF readout had failed to identify as toxic.

In a recent clinical study, administration of a 2′-*O*-methoxyethyl-modified AON targeting the sodium-glucose cotransporter 2 (herein SGLT2-MOE) resulted in increases in serum creatinine levels at the highest dose level with concomitant induction of other markers indicative of renal damage or dysfunction.[25] This SGLT2-MOE was demonstrated to be safe and effective in preclinical studies in several species.[7] These findings gave us the opportunity to challenge our in vitro assays with potentially toxic AON therapeutics of chemistries other than LNA. PTEC cells were exposed to SGLT2-MOE following the experimental scheme established for LNA-AONs (Figure 2A) with doses up to 500 μM. In accordance with the reported kidney liabilities in human, significant accumulation of EGF was detected in the supernatant of SGLT2-MOE-treated primary PTEC and PTEC-TERT1 (Figure 7B). KIM1 was elevated in PTEC-TERT1 but not in primary PTEC (Figure S14), consistent with the inferior predictability of KIM1 compared to EGF documented with LNA-AONs. These results suggest that the proposed in vitro screen is a promising strategy to advance AON therapeutics of various chemistries.

In light of the data presented here, we propose an EGF-based assay that can readily be implemented as an early safety screen in replacement of large-scale rat studies dedicated to identify nephrotoxicity

prior to clinical lead selection (Figure 7C). In summary, a library of AONs derived from in silico efficacy and safety prediction tools is applied to a confluent monolayer of PTEC-TERT1 without delivery assistance to mimic physiological conditions. Measurement of EGF in the cell supernatant serves as the principal toxicity biomarker and KIM-1 can be monitored as a complementary readout. AONs for which extracellular EGF and KIM-1 remain unchanged are prioritized for in vivo safety studies in rodents and non-human primates. Finally, further investigations of the EGF transcriptional signature in those cells and later on in AON-treated animals may unveil molecular biomarkers that could be translational.

## DISCUSSION

Antisense oligonucleotide (AON) drugs have already demonstrated therapeutic value for patients with cancer and metabolic diseases undergoing clinical trials.[26] However, the occurrence of renal failure in a healthy volunteer after the third dose of SPC5001, a locked nucleic acid (LNA)-modified AON, pointed out a crucial need to improve safety assessment of AON drug candidates prior to clinical trials. To date, safety profiling of AONs has typically relied on rodent studies with resource-, ethical-, and human-relevance matters. Here, we established a human cell model capable of recapitulating the renal toxicity caused by SPC5001 and a series of AONs poorly tolerated in vivo. We identified elevation of extracellular EGF as a robust in vitro biomarker of AON tubulotoxicity and uncovered the downregulation of EGFR signaling as central mode of toxicity of AONs in renal tubular cells. The in vitro assay described here predicts for the first time the kidney safety risk of AONs, and we propose its implementation as an early safety screen before in vivo studies are initiated.

Importantly, our mechanistic investigations revealed that the elevation of EGF levels in the supernatant of toxic AON-treated PTEC results from a progressive reduction of EGF uptake. Thus, the nature of EGF as an in vitro biomarker described here contrasts with the elevated expression of EGF observed upon kidney injury of distal tubule origin and may complicate its direct translation in the clinic given the abundance of circulating EGF in plasma and urine.[18] Notwithstanding, understanding the underlying mechanisms of inefficient EGF uptake may provide valuable insight toward identification of clinically translatable molecular biomarkers. To this end, we studied physical and functional interactions between AON, EGF, and EGFR. We found that the negative regulation of EGFR signaling is a central mode of toxicity of AONs in PTEC-TERT1. We further uncovered mechanisms of EGF/EGFR regulation that can contribute to the progressive accumulation of EGF in the supernatant of toxic AONs-treated cells. Acutely, toxic AONs promoted EGF-independent perinuclear accumulation of EGFR and transient downregulation of EGFR signaling, followed by blockage of an EGF transcriptional signature at 6 hr. At steady state, EGFR signaling and EGF uptake were diminished in toxic AONs-treated cells. It has been shown that gymnotically delivered AONs can largely localize in the perinuclear region of the cytoplasm, in distinct bodies that stain positive for markers of the late endosome.[27,28] Hypothetically, toxic AONs may distribute to the late endosome more prominently than innocuous AONs and interfere with proper trafficking and processing of endocytosed EGFR.

Beyond reporting a novel detection workflow to predict AON liabilities, our findings shed light on a yet unappreciated contribution of the EGFR signaling pathway to the cellular mechanisms of AON-induced cytotoxicity. EGFR is a central player in renal biology from development to homeostasis and injury repair.[18] Genetic and pharmacologic evidence have shown that EGFR activation in proximal tubular cells plays an important role in the recovery phase after acute kidney injury and that phospho-EGFR is the most markedly upregulated receptor tyrosine kinase in response to renal ischemia/reperfusion injury.[29] Downregulation of EGFR expression and activity after repeated injection of an unfavorable AON may cause tubular dysfunction and contribute to a negative outcome as other AON-induced cellular alterations come into play, such as lysosomal accumulation, off-target hybridization, and protein binding. Ultimately, organ function will depend on the cumulative tissue damage and the regenerative capacity of proximal tubular cells, and one can speculate that blockage of EGFR signaling by toxic AONs will pose a considerable hurdle to tissue repair. The physiological relevance of this mechanism, though, remains to be elucidated in rats and humans.

*Kim-1* was identified as the most highly upregulated protein in the renal proximal tubule 24 to 48 hr after ischemia in the rat and has since been associated with renal fibrosis, inflammation, and proximal tubular cell dedifferentiation.[30] The KIM-1 profile observed in our in vitro assays is intriguing in that AON-mediated cytotoxicity in human PTECs correlated mainly with decreases in KIM-1 levels except for the rare instances where extracellular EGF remained low. Multiple technical and biological reasons may account for the difficulty to reproduce the response of KIM-1 to kidney injuries in rat using cell models. Conventional cell culture conditions may not maintain a cellular state where the KIM-1 gene is adequately shut down and poised to positively respond to cellular stress and injuries. It will be relevant to address KIM-1 modulation in advanced human tissue-like models to re-evaluate its use as an in vitro biomarker and investigate a putative functional relationship between EGFR and KIM-1 and the translatability of this biomarker profile to the in vivo situation.

Overall, implementation of an EGF-based in vitro safety assessment of AONs prior to animal testing will have an immediate impact on the development of safer AON drugs. Future studies in rodents and higher species will indicate the usefulness of studying EGFR regulation as a predictor of AON-induced kidney damage and hopefully provide insights into the development of translational biomarkers.

## MATERIALS AND METHODS

### Chemistry of Single Strand Antisense Oligonucleotides

All tested antisense oligonucleotides (AONs) were 14–16 nucleotide-long gapmers with gap segments comprised of 2′-deoxynucleotides flanked by wing segments comprised of nucleotides with LNA sugar

modifications. Sequences and backbone modifications are provided in Table S2. The sequence and chemical modifications of SGLT2-MOE AON have been described previously.[25]

### Rodent Studies with AONs

#### *Kidney Toxicity Assessed in a 2-Week Rat Study*

Purpose-bred Wistar Han Crl:WI(Han) male rats obtained from Charles River Laboratories at 7–8 weeks of age were divided into groups of four (Table 1, value A) or eight (Table 1, value B) based on body weight and acclimatized for at least 5 days before dosing. The animals were group-housed under standard environmental conditions (22°C ± 2°C, relative humidity 50% ± 20%, a light/dark cycle 12 hr/12 hr, pelleted food and water ad libitum), were offered enriched environment in an Association for Assessment and Accreditation of Laboratory Animal Care International (AAALAC)-accredited facility and were regularly and carefully monitored. All procedures were conducted in strict adherence to the Swiss federal ordinance on animal protection and welfare, according to the rules of (AAALAC) and with the explicit approval of the local veterinary authority (Kantonales Veterinäramt Basel-Stadt, Switzerland). Test compounds were dosed subcutaneously at 40 mg/kg on days 1 and 8 at 2.5 mL/kg in the interscapular region. Control group animals received saline as vehicle control. On day 15, animals were orally administered tap water (10 mL/kg), and urine was collected on ice for 6 hr in metabolic cages. Urine protein levels (Aution Max AX-4280, ARKRAY) and urinary renal injury biomarkers were measured (Rat Kidney Toxicity Magnetic Bead Panel 2; Milliplex RKTX2MAG-37K, Millipore). Subsequently, on day 15, the rats were euthanized by an intraperitoneal injection of pentobarbital and exsanguinated. Kidney cortex samples were collected and fixed by immersion in 10% neutral buffered formalin, embedded in paraffin, sectioned to 5 μm and stained with H&E. The H&E sections were scanned at 20× magnification using an Aperio ScanScope AT (Leica Biosystems) scanner and pictures were captured via ImageScope software.

#### *Toxicity Assessed in a 2-Week Mouse Study: MYD88 Series*

C57BL/6JBom female mice (~20 g body weight), were obtained from Taconic Biosciences, divided into groups of five and acclimatized for at least 1 week before dosing. The animals were housed under standard conditions and were offered enriched environment. Test compounds were dosed intravenously at 15 mg/kg on days 1, 4, 8, 11, and 15 at 10 mL/kg. Groups were injected with saline as vehicle control. On day 17, animals were anaesthetized with 70% $CO_2$-30% $O_2$ before collection of blood from the retroorbital sinus. Macroscopic examination of liver and kidneys were performed and tissue weights recorded.

#### *Kidney Toxicity Assessed in a 1-Month Rat Study: BCL11a Series*

Wistar Hannover male rats (~180 g body weight), were obtained from Taconic, divided into groups of five and acclimatized for at least 1 week before dosing. The animals were group-housed under standard conditions and were offered enriched environment. Test compounds were dosed subcutaneously at 25 mg/kg on days 1, 8, 15, 22, and 29 at 10 mL/kg in the flank. One group was injected with saline as vehicle control. On day 31, animals were euthanized by cervical dislocation following anesthesia, blood was collected for serum creatinine, kidneys were weighed, and tissue was collected for histopathology and mRNA kidney biomarker analysis (kidney cortex in ice-cold mRNA later, then stored at 4°C).

All test compounds were formulated in isotonic sterile saline, sterile filtered (0.22 μm).

### PTEC Cultures, AON Treatment, and Cytotoxicity Assays

Primary PTEC (HRPTEpiC, #4100, ScienCell) and PTEC-TERT1 (RPTEC/TERT1, CHT-003-0002, Evercyte GmbH) were cultured according to the manufacturer's instructions in PTEC medium (DMEM/F12 without phenol red [110390-021, ThermoFisher Scientific]) containing 1% penicillin/streptomycin [GIBCO, 15140-122], 10 mM HEPES [GIBCO, 15630-056], 5.0 μg/mL human insulin [GIBCO, 41400-045], 5.0 μg/mL human transferrin [GIBCO, 41400-045], 8.65 ng/mL sodium selenite [GIBCO, 41400-045], 0.1 μM hydrocortisone [H6909, Sigma-Aldrich], 10 ng/mL human recombinant epidermal growth factor [236-EG-200, R&D Systems], 3.5 μg/mL ascorbic acid [Sigma-Aldrich, A4544 powder], 25 ng/mL prostaglandin E1 [Sigma-Aldrich, P5515], 3.2 pg/mL triiodo-L-thyronine [Sigma-Aldrich, T-5516], and 100 μg/mL Geneticin [GIBCO, 10131-027]).

For AON toxicity assessment, primary PTEC and PTEC-TERT1 were seeded into 96-well plates (353219, Corning) at a density of 40,000 and 20,000 cells/well respectively in PTEC medium and grown until confluence prior to treatment with AONs. LNA-AONs were dissolved in PBS and added to the cell culture at a final concentration of 1, 3, 10, 30, or 100 μM in a final volume of 100 μL. SGLT2-MOE-AON was dissolved in PBS and added to the cell culture at a final concentration of 30, 100, 300, 400, or 500 μM in a final volume of 100 μL. Medium was changed, stored at −20°C for kidney injury biomarker and cytokine analysis and refreshed along with AONs every 3 days. PBS served as vehicle control. Importantly, LNA-AON concentrations used in vitro approximate the concentration of LNA-AON detected in the renal cortex of cynomolgus monkeys after repeated dosing.[5] The later study reported renal concentrations of AON exceeding 2,500 mg/kg (~350 μM) after seven doses of LNA-AONs, associated with minimal degeneration of proximal tubule epithelial cells.

Cell viability was determined by measurement of intracellular ATP levels after 9 days of AON treatment using the CellTiter-Glo Luminescent Cell Viability Assay (G7571, Promega) according to manufacturer's instructions. For gene expression analysis, cells were collected in Panomics Lysis Mixture (QuantiGene Sample Processing Kit, QS0101, Affymetrix eBioscience) at day 6 of AON treatment unless otherwise indicated in the figure legends and stored at −80°C until analysis (described below). For cellular integrity, supernatants were collected at day 9 and measured for protease release using the CytoTox-Glo Cytotoxicity Assay (Promega, G9290) according to manufacturer's instructions. As positive control of drug-induced cell death, PTEC-TERT1 were treated with 30 and 100 μM

of Cyclosporine A (Sigma-Aldrich, C3662) for 24 hr. For apoptosis assay, cell lysates were prepared and monitored for caspases 3 and 7 activation at day 3 of AON exposure using the Caspase-GLO 3/7 assay kit (Promega, G8090) according to manufacturer's instructions. As positive control of drug-induced apoptosis, PTEC-TERT1 were treated with 1, 3, and 10 μM of Staurosporine (Sigma-Aldrich, S4400) for 24 hr.

Bright field images documenting PTEC-TERT1 morphological changes were taken at day 7 of AON treatment on living cells at 20× magnification. For cell count assessment at end point, cells exposed to AONs for 9 days were washed with PBS (GIBCO, 14190-094), fixed with 37°C-heated 4% paraformaldehyde (Alfa Aesar, 43368), permeabilized (4% cold-water fish gelatin [Sigma-Aldrich, G7041], 0.1% saponin [Sigma-Aldrich, 47036] in PBS) and stained with Phalloidin-Atto 488 (Sigma-Aldrich, 49409), 1:200 in staining buffer (4% cold-water fish gelatin, 0.01% saponin in PBS), and DAPI (Sigma-Aldrich, D9542, 1 mg/mL). Image acquisition was performed on 6 wells per conditions (35–65 fields per well) using the Operetta high content imager (PerkinElmer) at 20× magnification and analyzed using Harmony software (PerkinElmer).

#### Human Hepatocytes and Retinal Pigment Epithelial Cells

Cryopreserved human hepatocytes were suspended in William's Medium E (WME) without phenol red (Sigma-Aldrich, W-1878) supplemented with 10% fetal calf serum, penicillin (100 U/mL), and streptomycin (0.1 mg/mL) at a density of approximately $5 \times 10^6$ cells/mL and seeded into collagen-coated 96-well plates (Becton Dickinson AG) at a density of 40,000 cells/well. Cells were pre-cultured for 3–4 hr allowing for attachment to cell culture plates before start of treatment with AONs. Seeding medium was replaced by 90 μL of serum-free WME, and 10 μL of AON stock solutions in PBS were added to the cell culture and left on the cells for 3 days, before EGF levels in the supernatant and cellular ATP levels were determined as described for PTEC-TERT1.

The retinal pigment epithelial cell line ARPE-19 (CRL-2302, ATCC) was cultivated according to manufacturer's instructions in ARPE-19 medium (ATCC 30-2006). Cells were seeded into 96-well plates at 20,000 cells per well. AON treatment was performed at confluency in ARPE-19 medium supplemented with 5 ng/mL of EGF and intracellular ATP was measured at day 7 as described for PTEC-TERT1.

#### EGF and Cytokine Profiling by Luminex-Based ELISA

For kidney injury biomarker and cytokine profiling shown in Figures 2B and S2, supernatants were thawed on ice, diluted 1:2 and 1:10 in sample dilution buffer (M60-009RDPD, BioRad), and analyzed by multiplex ELISA using Human Kidney Tox Panel I (Bio-plex,171-ATR1CK, analytes: calbindin, clusterin, GST-π, IL-18, KIM-1, MCP-1), Human Kidney Tox Panel II (Bio-plex,171-ATR2CK, analytes: albumin, beta2 microglobulin, cystatin C, NGAL, OPN, TFF3), and Human Cytokine and Chemokine Panel (Milliplex, HCYTOMAG-60K-PX30, analytes: EGF, G-CSF, GM-CSF, IFN-α2, IFN-γ, IL-1α, IL-1β, IL-1ra, IL-2, IL-3, IL-4, IL-5, IL-6, IL-7, IL-8, IL-10, IL-12 [p40], IL-12 [p70], IL-13, IL-15, IL-17, IP-10, MCP-1, MIP-1α, MIP-1β, TNF-α, TNF-β, VEGF, RANTES, and eotaxin/CCL11) followed by analysis using the Bio-Plex 200 Systems (BioRad) according to manufacturer's instructions. For analysis of human EGF and KIM-1 from Figures 2D, 3, 4, 5, 6, and 7, supernatants were thawed on ice, diluted 1:2 and 1:10 in sample dilution buffer (BioRad, M60-009RDPD), and analyzed by multiplex ELISA using Human Kidney Injury Panel 4 (Millipore, HKI4MAG-99K). Mean concentrations and SDs of triplicate wells were calculated and normalized on vehicle control.

#### Gene Expression Analysis

Cells grown in 96-well plates format were collected by replacing culture medium with 100 μL/well of 1× RNA lysis mixture (QuantiGene Sample Processing Kit, QS0101). RNA lysis mixtures were kept at −80°C until analysis. A total of 20 μL of lysates were mixed with mRNA-capture magnetic beads sets (Panomics QuantiGene Plex Sets, 12697 and 12812), incubated overnight, processed for branched DNA amplification, and analyzed according to manufacturer's instructions (Panomics QuantiGene Plex Assay kit, QP1015). The PPIB probe was used as housekeeping gene for normalization. Average fluorescence intensity (FI) and SD of three biological replicates were calculated and normalized on vehicle control.

#### EGF Consumption

The medium of confluent PTEC-TERT1 maintained in 96-well plates as described above was replaced with fresh PTEC medium, and 10 μL of supernatant was collected after 8, 24, 48, and 72 hr for EGF analysis by Luminex ELISA. Six wells were devoid of cells and served as no-cell control to account for EGF stability over time at 37°C. Data are reported as EGF concentration in the supernatant of PTEC-TERT1 normalized on the no-cell control at the corresponding time point.

#### Western Blot Analysis

PTEC-TERT1 cells were plated at 500,000 cells/well in 6-well plates in PTEC medium and grown until confluency prior to AON treatment and protein analysis. For steady-state experiments, cells were exposed to 100 μM of AONs as described above for human PTEC, incubated for 24 and 72 hr, respectively, washed with cold PBS, and lysed in 100 μL of ice-cold RIPA buffer (60 mM Tris-HCl at pH 7.4, 150 mM NaCl, 0.25% SDS, 1% NP40, 1× PhosSTOP [04906845001, Roche Diagnostics] and 1× Complete protease inhibitor [Roche, 04693124001]). To measure effects of non-AON nephrotoxicant, PTEC-TERT1 were treated with 10 μM of cyclosporine A for 24 hr prior to lysis as described above. For acute experiments (Figure 5D, 10 min), cells were incubated in PTEC medium without EGF for an overnight period followed by exposure to 100 μM AONs or vehicle in PTEC medium containing 10 ng/mL of EGF. Plates were transferred on ice after 10 min of AON and EGF exposure, washed with cold PBS, and lysed in 100 μL of ice cold RIPA buffer. Protein content in cell lysis was measured by BCA Kit (ThermoFisher, 23225), and 20 μg of total proteins were separated by electrophoresis using a 5%–20% polyacrylamide gel. Western blot analyses was carried out using the following antibodies: phospho-Akt-Ser473 (Cell

Signaling, 4060, 1:1,000), phospho-Erk1/2-Thr202/Tyr204 (Cell Signaling, 4370, 1:2,000), and GAPDH (Sigma-Aldrich, G8795, 1:2,000). The CHEMIDOC MP Imaging System (BioRad) was used to scan the membranes.

#### PTEC-TERT1 Treatment with Cetuximab and Erlotinib

PTEC-TERT1 were seeded into 96-well plates (Corning, 353219) at a density of 20,000 cells/well in PTEC medium and grown until confluence prior to treatment. Compounds and vehicle controls were diluted in PTEC medium along with AONs and added to cells according to the experimental layout in Figure 1A. The following final concentrations were used: 50, 250, and 500 μg/mL cetuximab (Merk Serono, 5 mg/mL in 0.9% NaCl) and 5 μM Erlotinib (sc-202154, Santa Cruz Biotechnology). EGF was measured at day 6 and ATP at day 9 as described above.

#### Surface Plasmon Resonance

Surface plasmon resonance (SPR) experiments were performed on the BiaCore instruments 3000 and 2000 (GE Healthcare, Uppsala, Sweden) at 25°C. PBS buffer composed of 10 mM phosphate, 137 mM NaCl, and 27 mM KCl with or without 0.05% P20 (w/v), pH 7.4 was used as running buffer to perform protein immobilization and binding assays. Prior to SPR analysis, the running buffer was filtered with ExpressPlus steritop filters with 0.22 μm cut off (Millipore) and degassed. Immobilization and binding assays were performed at flow rate of 5 or 50 μL/min, respectively.

Tris-NTA-biotin conjugate (Biotechrabbit GmbH) was captured on streptavidin pre-coated SA sensors (GE Healthcare, BR-1000-32). First, streptavidin sensor was conditioned with three consecutive 1-min injections of high salt solution in sodium hydroxide (50 mM NaOH, 1 M NaCl). Next, Tris-NTA-biotin stock solution (1 mg/mL) was diluted 100× in running buffer and applied over the streptavidin sensor surface to achieve saturated immobilization levels of Tris-NTA of ∼400–500 resonance units (RUs). Finally, free biotin solution (10 μM in running buffer) was injected once (1 min) over the sensor surface to block remaining binding sites of streptavidin. EGFR receptor (ectodomain, residues 1–645, ThermoFisher, 10001-H08H-250) was captured on Tris-NTA- modified sensor surface as follows: first, Tris-NTA sensor was conditioned with three consecutive 1 min injections of 350 mM EDTA in distilled water and contacted with a solution of 500 μM $NiCl_2$ (1 min injection); next, human EGFR was diluted in running buffer to 5 μg/mL and applied over Tris-NTA sensor surface to achieve EGFR immobilization levels of ∼400 RU. EGF peptide (Sigma-Aldrich, E9644) was titrated up to 1 μM over EGFR surface in triplicates. Affinity of EGF to EGFR was estimated to be 40 nM (±3.7 nM) (data not shown). For competition experiments, EGF (500 nM) and AONs (5 μM) were analyzed separately in solution or in a mixture (500 nM EGF and 5 μM AON). Buffer injections were performed as negative controls. Each sample was analyzed in triplicates.

#### EGF Uptake and EGFR Internalization by Confocal Imaging

For the EGF/EGFR binding assay (Figure 5A), cells were incubated in PTEC medium without EGF for an overnight period, washed with room temperature PBS (GIBCO, 14190-094), incubated for 5 min in PBS, followed by a 10-min incubation on ice with 100 μM of AONs and 10 ng/mL EGF-488 (ThermoFisher, E13345) in EGF-free cold PTEC medium. Cells were washed in cold PBS, fixed with cold 4% paraformaldehyde for 15 min (Alfa Aesar, 43368), and washed again three times with PBS. For the EGF uptake assay shown in Figure 5B, the same steps were performed except that all reagents were kept at room temperature and incubation with AONs and EGF-488 was done at 37°C. For both assays, the control with cetuximab was performed by adding 100 μg/mL of cetuximab (Merck Serono) 5 min prior to and during exposition to EGF-488 and AONs. Fixed cells were permeabilized using 4% cold-water fish gelatin (Sigma-Aldrich, G7041) and 0.1% saponin (Sigma-Aldrich, 47036) in PBS for 10 min at room temperature and immuno-labeled with anti-EGFR (2E9, Abcam, ab8465, 1:200 in staining buffer [4% cold cold-water fish gelatin (Sigma-Aldrich, G7041) and, 0.01% saponin (Sigma-Aldrich, 47036) in PBS]) followed by anti-mouse IgG-Alexa Fluor 647 antibody (ThermoFisher, A31571 in staining buffer) and stained with DAPI (Sigma-Aldrich, D9542, 1 mg/mL, 1:1,000). Five images of randomly selected field of view per biological triplicates were acquired on a laser-scanning confocal microscope (Leica TCS SP8) using a 63× objective. Settings were adjusted to maximize dynamic range and reduce pixel saturation (pixel size: 120.56 nm × 120.56 nm; image size: 1,024 × 1,024; bit depth: 12 bit; number of z sections: 5).

For EGF uptake shown in Figure 3D, the same procedure was applied except that PTEC-TERT1 were exposed to 100 μM AONs for 6 days prior to EGF uptake assay and AONs were not added during the 10 min incubation with EGF-488. The number of EGF foci and nuclei per field was determined using the ImageJ image processing program.

#### Quantification of EGFR Internalization and Statistical Analysis

Quantification of EGFR intensity within an arbitrarily defined area around the nucleus was performed based on a particle tracking method introduced by Balzarini and Koumoutsakos.[31] Four steps, as elaborated in the original publication, were implemented. First, in order to correct for the uneven background intensity, image restoration was performed by using boxcar average over a square region with a user-defined parameter-radius. Second, point locations were estimated by finding local intensity maxima under the condition that the intensity value should be higher than a user-defined absolute intensity value. Third, the point locations were further refined by calculating the offset from the brightness-weighted centroid. Fourth, non-particle discrimination was used to reject spurious detection such as dust or particle aggregates. In fact this parameter was set as zero in our detection because particle aggregates were aimed to be kept. In addition, two modifications from the original algorithm were implemented to better fit this work. First, the level of radius was adapted to detect both large EGFR particles with a 5-pixel radius and small particles with a 2-pixel radius. Second, an adaptive intensity threshold based on the distribution of the control image was used to overcome the inter-plate variability. The threshold was set to 1.5 SDs

above the mean. After detection, EGFR particles were assigned to the nearest nuclei. The following quantification was then performed per nucleus: (1) a perinuclear area was defined as 50% larger than the nucleus radius, (2) the number and size in pixel of EGFR foci in the perinuclear area per cell were calculated, and (3) the summed intensities of large EGFR (greater than five pixels) in the perinuclear area per cell were calculated and named as i.EFGR_50%_big_sum. The mean fluorescence intensity reflects the total perinuclear EGFR intensity level regardless of the number of particles.

For statistical analysis, a generalized least-squares model (a weighted linear regression) was fit to the data (n = 1,117). Specifically, the readout i.EFGR_50%_big_sum was log-transformed and regressed on treatment and interactions of treatment and cetuximab status (Yes/No binary variable). The model was validated by means of residual analysis, checking independence from dependent variable and homogeneity of variances with regards to independent variables, as well as overall normal distribution of residuals.

#### Quantification of EGF Uptake by Flow Cytometry

Eighty percent confluent PTEC-TERT1 were incubated overnight in PTEC medium without EGF, harvested with 0.25% Trypsin (GIBCO, 25200-056), centrifuged at 220 × *g* for 5 min, and distributed at 150–200,000 cells per tube in PTEC medium without EGF with or without 100 ug/mL of cetuximab for 5 min at 37°C. Cells were incubated for 10 min at 37°C in EGF-free or EGF-488-containing (10 ng/mL) PTEC medium with or without cetuximab and 100 μM AONs as indicated in figure legends. Cells were re-suspended in ice-cold running buffer (MACSQuant, 130-092-747) and analyzed by flow cytometry on a MACSQuant VYB (Miltenyi Biotec). The data of at least 10,000 cells per condition were analyzed with FlowJo v10 software and reported as cell number relative to EGF-488 fluorescence intensity.

#### Molecular Phenotyping: EGF Transcriptional Signature

PTEC-TERT1 were exposed to 10, 30, and 100 μM of AONs in EGF-containing (10 ng/mL) or EGF-free PTEC medium. After 6 hr of treatment, cells were lysed, total RNA was extracted, and pathway reporter genes were quantified following procedures described before.[23] Each condition was tested in three biological replicates. Using vehicle controls with and without EGF, we identified 66 EGF-signature genes in PTEC-TERT1 by using the R/Bioconductor software package *edgeR* and the following threshold: $\geq 8$ reads per million reads in an average sequencing run, absolute $\log_2$ fold change $\geq 0.5$, and Benjamini-Hochberg (BH) adjusted p value of differential expression no larger than 0.05.

We performed functional enrichment analysis of the 66 EGF-signature genes with biological processes defined in Gene Ontology and biological pathways encoded in KEGG using the DAVID.[32] We identified 115 significantly enriched gene sets (BH-adjusted $p < 0.05$) that can be divided into 22 clusters based on composition similarity. The gene sets with the lowest p value of enrichment in each cluster are shown. EGF-dependent regulation of EGF-signature genes in different AON treatments were quantified by EGF response scores, which are defined as $|\log_{10}(pValue)|$*sign($log_2FC$), namely absolute log-10-transformed p values reported by *edgeR* multiplied by the sign of the log-2-transformed fold change. A positive (negative) score of gene *G* in AON *X* treatment indicates that *G* is higher (lower) expressed when AON *X* is applied to cells in the presence of EGF than in its absence.

#### General Statistical Analysis

Unless otherwise stated in the Materials and Methods and figure legends, statistical analysis was carried out by ANOVA using Dunnett's multiple comparison test at 95% confidence interval and alpha of 0.05. AON treatments were analyzed against the vehicle control of similar conditions unless otherwise stated in the figure legends; p values were adjusted to account for multiple comparisons. n indicates number of biological replicates, i.e., cells from different well plates and passages.

## SUPPLEMENTAL INFORMATION

Supplemental Information includes fourteen figures and two tables and can be found with this article online at http://dx.doi.org/10.1016/j.omtn.2016.11.006.

## AUTHOR CONTRIBUTIONS

A. Moisan conceived the study, supervised experiments, analyzed the data, and wrote the manuscript; M.G. supervised experiments in primary PTEC; J.D.Z. performed data analysis of molecular phenotyping and participated in manuscript writing; Y.T. and K.D.E. performed post-hoc analysis of rodent studies and participated in manuscript writing; S.S. supervised experiments in hepatocytes; R.G. and B.A. executed in vitro experiments; S.H. supervised SPR experiments; F.B. and X.C. performed image-based quantification of perinuclear EGFR; A. Maunz performed data analysis of perinuclear EGFR; R.V. supervised EGF uptake experiments; A.B.-B. performed histopathological evaluation of rat kidney; M.F. coordinated and analyzed rat studies; T.S., F.S., and A.B.R. revised and approved the manuscript.

## CONFLICTS OF INTEREST

All authors are employees of F. Hoffmann-La Roche. The funder provided support in the form of salaries for authors but did not have any additional role in the study design, data collection and analysis, decision to publish, or preparation of the manuscript. A. Moisan, J.D.Z., and F.B. are non-voting shareholders of F. Hoffmann-La Roche. A. Moisan, M.G., S.S., and A.B.R. are named inventors on patent applications EP16174996.5 and EP16174994.0. This does not alter our adherence to policies on sharing data and materials.

## ACKNOWLEDGMENTS

The authors thank Laurence Hilfiger, Tanja Minz, Erich Kueng, and Melanie Hug for technical support, Marco Berrera for help with molecular phenotyping analysis, Marianne Bonde Mogensen for synthesis of SGLT2-MOE AON, Ludovic Collin for access to imaging facilities, Kimberley Homan and Marianne Rudolph Hanson for critical

reading of the manuscript, and Erich Koller, Ulrich Certa, Andreas Dieckman, and Martin Ebeling for insightful discussions. R.V. was supported by the Roche Postdoctoral Fellowship (RPF) program.

## REFERENCES


1. Deleavey, G.F., and Damha, M.J. (2012). Designing chemically modified oligonucleotides for targeted gene silencing. Chem. Biol. *19*, 937–954.
2. Henry, S.P., Kim, T.W., Kramer-Stickland, K., Zanardi, T.A., Fey, R.A., and Levin, A.A. (2007). Toxicologic properties of phosphorothioate 2′−O-methoxyethyl chimeric antisense inhibitors in animals and man. In Antisense Drug Technology. Principles, Strategies and Applications, S.T. Crooke, ed. (CRC Press), pp. 327–364.
3. Voit, T., Topaloglu, H., Straub, V., Muntoni, F., Deconinck, N., Campion, G., De Kimpe, S.J., Eagle, M., Guglieri, M., Hood, S., et al. (2014). Safety and efficacy of drisapersen for the treatment of Duchenne muscular dystrophy (DEMAND II): an exploratory, randomised, placebo-controlled phase 2 study. Lancet Neurol. *13*, 987–996.
4. Herrington, W.G., Talbot, D.C., Lahn, M.M., Brandt, J.T., Callies, S., Nagle, R., Winearls, C.G., and Roberts, I.S. (2011). Association of long-term administration of the survivin mRNA-targeted antisense oligonucleotide LY2181308 with reversible kidney injury in a patient with metastatic melanoma. Am. J. Kidney Dis. *57*, 300–303.
5. Henry, S.P., Johnson, M., Zanardi, T.A., Fey, R., Auyeung, D., Lappin, P.B., and Levin, A.A. (2012). Renal uptake and tolerability of a 2′-O-methoxyethyl modified antisense oligonucleotide (ISIS 113715) in monkey. Toxicology *301*, 13–20.
6. Monteith, D.K., Horner, M.J., Gillett, N.A., Butler, M., Geary, R., Burckin, T., Ushiro-Watanabe, T., and Levin, A.A. (1999). Evaluation of the renal effects of an antisense phosphorothioate oligodeoxynucleotide in monkeys. Toxicol. Pathol. *27*, 307–317.
7. Zanardi, T.A., Han, S.C., Jeong, E.J., Rime, S., Yu, R.Z., Chakravarty, K., and Henry, S.P. (2012). Pharmacodynamics and subchronic toxicity in mice and monkeys of ISIS 388626, a second-generation antisense oligonucleotide that targets human sodium glucose cotransporter 2. J. Pharmacol. Exp. Ther. *343*, 489–496.
8. Kakiuchi-Kiyota, S., Whiteley, L.O., Ryan, A.M., and Mathialagan, N. (2015). Development of a method for profiling protein interactions with LNA-modified antisense oligonucleotides using protein microarrays. Nucleic Acid Ther. *26*, 93–101.
9. Burel, S.A., Hart, C.E., Cauntay, P., Hsiao, J., Machemer, T., Katz, M., Watt, A., Bui, H.H., Younis, H., Sabripour, M., et al. (2016). Hepatotoxicity of high affinity gapmer antisense oligonucleotides is mediated by RNase H1 dependent promiscuous reduction of very long pre-mRNA transcripts. Nucleic Acids Res. *44*, 2093–2109.
10. Kamola, P.J., Kitson, J.D., Turner, G., Maratou, K., Eriksson, S., Panjwani, A., Warnock, L.C., Douillard Guilloux, G.A., Moores, K., Koppe, E.L., et al. (2015). In silico and in vitro evaluation of exonic and intronic off-target effects form a critical element of therapeutic ASO gapmer optimization. Nucleic Acids Res. *43*, 8638–8650.
11. Janssen, H.L., Kauppinen, S., and Hodges, M.R. (2013). HCV infection and miravirsen. N. Engl. J. Med. *369*, 878.
12. van Poelgeest, E.P., Swart, R.M., Betjes, M.G., Moerland, M., Weening, J.J., Tessier, Y., Hodges, M.R., Levin, A.A., and Burggraaf, J. (2013). Acute kidney injury during therapy with an antisense oligonucleotide directed against PCSK9. Am. J. Kidney Dis. *62*, 796–800.
13. van Poelgeest, E.P., Hodges, M.R., Moerland, M., Tessier, Y., Levin, A.A., Persson, R., Lindholm, M.W., Dumong Erichsen, K., Ørum, H., Cohen, A.F., and Burggraaf, J. (2015). Antisense-mediated reduction of proprotein convertase subtilisin/kexin type 9 (PCSK9): a first-in-human randomized, placebo-controlled trial. Br. J. Clin. Pharmacol. *80*, 1350–1361.
14. Lindholm, M.W., Hansen, H.F., and Tessier, Y. (2013). LNA Oligonucleotide. In Vivo Screening v2.0 (Hørsholm, Denmark: Santaris Pharma A/S).
15. Geary, R.S., Norris, D., Yu, R., and Bennett, C.F. (2015). Pharmacokinetics, biodistribution and cell uptake of antisense oligonucleotides. Adv. Drug Deliv. Rev. *87*, 46–51.
16. Ichimura, T., Bonventre, J.V., Bailly, V., Wei, H., Hession, C.A., Cate, R.L., and Sanicola, M. (1998). Kidney injury molecule-1 (KIM-1), a putative epithelial cell adhesion molecule containing a novel immunoglobulin domain, is up-regulated in renal cells after injury. J. Biol. Chem. *273*, 4135–4142.
17. Bonventre, J.V. (2009). Kidney injury molecule-1 (KIM-1): a urinary biomarker and much more. Nephrol. Dial. Transplant. *24*, 3265–3268.
18. Zeng, F., Singh, A.B., and Harris, R.C. (2009). The role of the EGF family of ligands and receptors in renal development, physiology and pathophysiology. Exp. Cell Res. *315*, 602–610.
19. Li, S., Schmitz, K.R., Jeffrey, P.D., Wiltzius, J.J., Kussie, P., and Ferguson, K.M. (2005). Structural basis for inhibition of the epidermal growth factor receptor by cetuximab. Cancer Cell *7*, 301–311.
20. Sewing, S., Boess, F., Moisan, A., Bertinetti-Lapatki, C., Minz, T., Hedtjaern, M., Tessier, Y., Schuler, F., Singer, T., and Roth, A.B. (2016). Establishment of a predictive in vitro assay for assessment of the hepatotoxic potential of oligonucleotide drugs. PLoS ONE *11*, e0159431.
21. Rockwell, P., O'Connor, W.J., King, K., Goldstein, N.I., Zhang, L.M., and Stein, C.A. (1997). Cell-surface perturbations of the epidermal growth factor and vascular endothelial growth factor receptors by phosphorothioate oligodeoxynucleotides. Proc. Natl. Acad. Sci. USA *94*, 6523–6528.
22. Guvakova, M.A., Yakubov, L.A., Vlodavsky, I., Tonkinson, J.L., and Stein, C.A. (1995). Phosphorothioate oligodeoxynucleotides bind to basic fibroblast growth factor, inhibit its binding to cell surface receptors, and remove it from low affinity binding sites on extracellular matrix. J. Biol. Chem. *270*, 2620–2627.
23. Zhang, J.D., Küng, E., Boess, F., Certa, U., and Ebeling, M. (2015). Pathway reporter genes define molecular phenotypes of human cells. BMC Genomics *16*, 342.
24. Zhang, J.D., Schindler, T., Küng, E., Ebeling, M., and Certa, U. (2014). Highly sensitive amplicon-based transcript quantification by semiconductor sequencing. BMC Genomics *15*, 565.
25. van Meer, L., Moerland, M., van Dongen, M., Goulouze, B., de Kam, M., Klaassen, E., Cohen, A., and Burggraaf, J. (2016). Renal effects of antisense-mediated inhibition of SGLT2. J. Pharmacol. Exp. Ther. *359*, 280–289.
26. Moreno, P.M., and Pêgo, A.P. (2014). Therapeutic antisense oligonucleotides against cancer: hurdling to the clinic. Front Chem. *2*, 87.
27. Castanotto, D., Lin, M., Kowolik, C., Wang, L., Ren, X.Q., Soifer, H.S., Koch, T., Hansen, B.R., Oerum, H., Armstrong, B., et al. (2015). A cytoplasmic pathway for gapmer antisense oligonucleotide-mediated gene silencing in mammalian cells. Nucleic Acids Res. *43*, 9350–9361.
28. Koller, E., Vincent, T.M., Chappell, A., De, S., Manoharan, M., and Bennett, C.F. (2011). Mechanisms of single-stranded phosphorothioate modified antisense oligonucleotide accumulation in hepatocytes. Nucleic Acids Res. *39*, 4795–4807.
29. Chen, J., Chen, J.K., and Harris, R.C. (2012). Deletion of the epidermal growth factor receptor in renal proximal tubule epithelial cells delays recovery from acute kidney injury. Kidney Int. *82*, 45–52.
30. van Timmeren, M.M., van den Heuvel, M.C., Bailly, V., Bakker, S.J., van Goor, H., and Stegeman, C.A. (2007). Tubular kidney injury molecule-1 (KIM-1) in human renal disease. J. Pathol. *212*, 209–217.
31. Sbalzarini, I.F., and Koumoutsakos, P. (2005). Feature point tracking and trajectory analysis for video imaging in cell biology. J. Struct. Biol. *151*, 182–195.
32. Huang, W., Sherman, B.T., and Lempicki, R.A. (2009). Systematic and integrative analysis of large gene lists using DAVID bioinformatics resources. Nat. Protoc. *4*, 44–57.